Mixed-Conducting Dense Ceramics for Gas Separation Applications*

U. Balachandran, B. Ma, J. Guan,† P. S. Maiya, J. T. Dusek,
J. J. Picciolo, and S. E. Dorris
Energy Technology Division
Argonne National Laboratory
Argonne, Illinois 60439 USA

M. Liu
School of Materials Science and Engineering
Georgia Institute of Technology
Atlanta, Georgia 30332 USA

June 1999

Invited manuscript submitted for publication in Proceedings of Symposium on Solid State Ionic Devices, 195th Meeting of the Electrochemical Society, May 2-7, 1999, Seattle.

*Work supported by the U.S. Department of Energy, Federal Energy Technology Center, under Contract W-31-109-Eng-38.

---

†Current Address: AlliedSignal Inc., Aerospace Equipment Systems, Torrance, CA 90504.

DISCLAIMER

MIXED-CONDUCTING DENSE CERAMICS FOR GAS SEPARATION APPLICATIONS

U. Balachandran,‡ B. Ma, J. Guan,† P. S. Maiya, J. T. Dusek,
J. J. Picciolo, and S. E. Dorris
Energy Technology Division, Argonne National Laboratory
Argonne, Illinois 60439 USA

M. Liu
School of Materials Science and Engineering, Georgia Institute of Technology
Atlanta, Georgia 30332 USA

ABSTRACT

Mixed-conducting (electronic and ionic conducting) dense ceramics are used in many applications, including fuel cells, gas separation membranes, batteries, sensors, and electrocatalysis. This paper describes mixed-conducting ceramic membranes that are being developed to selectively remove oxygen and hydrogen from gas streams in a nongalvanic mode of operation (i.e., with no electrodes or external power supply). Ceramic membranes made of Sr-Fe-Co oxide (SFC), which exhibits high combined electronic and oxygen ionic conductivities, can be used for high-purity oxygen separation and/or partial oxidation of methane to synthesis gas (syngas, a mixture of CO and H_2). The electronic and ionic conductivities of SFC were found to be comparable in magnitude. Steady-state oxygen permeability of SFC has been measured as a function of oxygen-partial-pressure gradient and temperature. For a ≈3-mm-thick membrane, the oxygen permeability was ≈2.5 $scc \cdot cm^{-2} \cdot min^{-1}$ at 900°C. Oxygen permeation increases as membrane thickness decreases. Tubular SFC membranes have been fabricated and operated at 900°C for ≈1000 h in converting methane into syngas. The oxygen permeated through the membrane reacted with methane in the presence of a catalyst and produced syngas.

We also studied the transport properties of yttria-doped $BaCeO_{3-\delta}$ (BCY) by impedance spectroscopy and open-cell voltage (OCV) measurement. Total conductivity of the BCY sample increased from ≈5 x 10^{-3} $\Omega^{-1} \cdot cm^{-1}$ to ≈2 x 10^{-2} $\Omega^{-1} \cdot cm^{-1}$, whereas the protonic transference number decreased from 0.87 to 0.63 and the oxygen transference number increased from 0.03 to 0.15 as temperature increased from 600 to 800°C. Unlike SFC, in which the ionic and electronic conductivities are nearly equivalent, BCY exhibits protonic conductivity that is significantly higher than its electronic conductivity. To enhance the electronic conductivity and therefore to increase hydrogen permeation, metal powder was combined with the BCY to form a cermet membrane. Nongalvanic permeation of hydrogen through the BCY-cermet membranes was demonstrated and characterized as a function of membrane thickness.

---

‡Corresponding Author. Tel: (630)252-4250, Fax: (630)252-3604, e-mail: balu@anl.gov
†Current Address: AlliedSignal Inc., Aerospace Equipment Systems, Torrance, CA 90504.

INTRODUCTION

In recent years, mixed-conducting oxides, in which both ionic and electronic charge carriers exist, have received increased attention because of their technological importance in high-temperature electrochemical devices and in electrocatalysis. For example, they are used as sensors and as electrodes in solid-state fuel cells; if their ionic conductivities are high enough, they can be used as dense membranes for gas separation. The development of cost-effective membrane-based reactor and separation technologies is of considerable interest for applications in advanced coal-based power and fuel technologies. Concerns over global climate change are driving nations to reduce carbon dioxide emissions. Hydrogen is considered the fuel of choice for both electric power and transportation industry because of the potential for reducing the generation of harmful SO_x and NO_x. Membrane technologies may lower the process cost by integrating hydrogen separation and purification into the shift conversion process and by converting hydrogen from streams for which recovery is not currently economical due to low concentration, low pressure, or other factors. On the other hand, oxygen separation using mixed-conducting membranes also has great potential for meeting the needs of many segments of the oxygen market. These envisioned applications range from small-scale oxygen pumps for medical applications to large-scale usage in methane conversion and combustion processes such as coalliquefaction.

In the early 1980s, Iwahara et al. [1-3] first reported protonic conduction in $SrCeO_3$ materials. Later, the $BaCeO_3$ system was extensively studied because of its higher conductivities [4-7]. Following their discovery by Teraoka et al. [8,9] in the late 1980s, mixed-conducting perovskites with combined electronic and oxide ionic conductivities and appreciable oxygen permeability were investigated [10-15]. Recently, Balachandran et al. [16,17] showed that nonperovskite $SrFeCo_{0.5}O_x$ (SFC) exhibits not only higher combined electronic and oxygen ionic conductivities but also structural stability. The electronic and oxygen ionic conductivities of this material are comparable in magnitude; this makes it a unique material. Oxygen permeation flux of dense SFC membranes is superior to that observed in other oxides. Extruded SFC tubular membranes have been evaluated in a methane conversion reactor operating at ≈900°C to convert methane to syngas in the presence of a reforming catalyst. Methane conversion coefficients of >98% were observed [18,19], and the reactor tubes have been operated for ≈1000 h.

Unlike SFC, protonic conductors normally have much higher ionic conductivity than electronic conductivity; the hydrogen permeation rate is therefore limited by the low electronic conductivity of these materials. We have recently developed composite hydrogen permeation membranes derived from high proton-conducting yttria-doped $BaCeO_{3-\delta}$ (BCY) materials. The hydrogen permeation rate of the composite BCY membranes has been significantly improved.

In this paper, we report our recent results on the oxygen-permeable SFC membranes and hydrogen-permeable BCY composite membranes. SFC and BCY materials were characterized at elevated temperatures in various environments. Electronic and oxygen ionic conductivities of SFC were measured by conventional and electron-blocking 4-probe methods. Oxygen stoichiometry was characterized with thermogravimetric analysis. Oxygen chemical diffusion coefficient was determined in the time-relaxation experiments from change of conductivity and/or weight of the specimen after suddenly switching the surrounding gas environment. Oxygen permeation flux was measured as a function of

differential oxygen partial pressure (Δp_{O_2}) and temperature. Oxygen permeation data from methane conversion reactor was compared with the steady-state oxygen permeation data obtained with a gas-tight electrochemical cell.

Conductivity of BCY material was characterized with the two-probe technique from impedance spectroscopy (IS). Open-cell voltages (OCVs) of BCY were measured in various gas environments (cell configurations) and used to derive the electronic and ionic transference numbers. The hydrogen permeation rate through a BCY-cermet membrane was studied as a function of membrane thickness to determine the relative importance of bulk and interfacial properties.

EXPERIMENT

Oxygen-permeable SFC samples were prepared by a solid-state reaction method, with $SrCO_3$, Fe_2O_3, and $Co(NO_3)_2 \cdot 6H_2O$ as starting materials. Mixing and grinding were performed in isopropanol with zirconia media. After drying, the mixtures were calcined at ≈850°C for 16 h in air with intermittent grinding. Phase purity was confirmed by X-ray diffraction (XRD). The resultant powders were pressed into pellets under 120 MPa load and sintered in air at 1200°C for 5 h. Bar specimens cut from the sintered pellets were used for measuring conductivity and for determination of the chemical diffusion coefficient. Both sides of the sintered pellets were polished using 600-grade SiC paper and used for permeation tests. Proton-conducting BCY was prepared by mixing appropriate amounts of $BaCO_3$, CeO_2, and Y_2O_3 and then calcining the mixture at 1000°C for 12 h in air. The resulting powder was ball-milled and recalcined at 1200°C for 10 h in air. BCY samples were prepared by pressing the BCY powder with a 100 MPa load into green-body pellets of 22.5 mm diameter, followed by sintering in air at 1550°C for 10 h. In making the BCY-cermet samples, an appropriate amount of metal powder

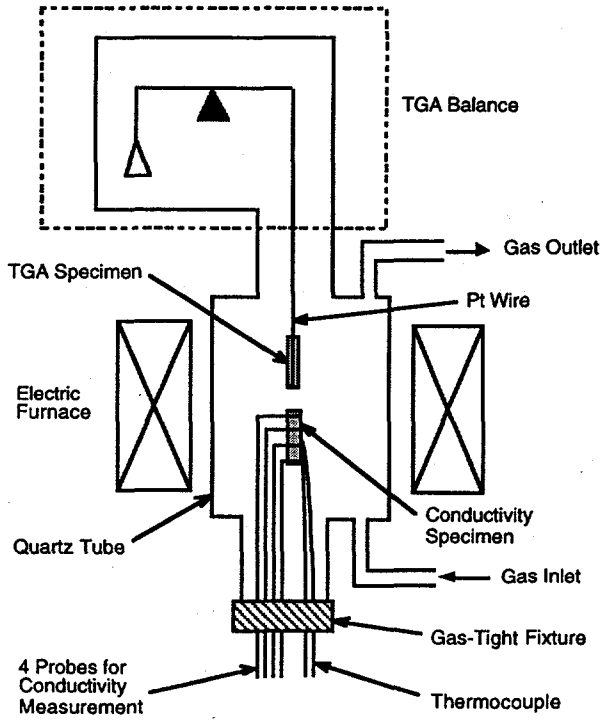

Figure 1. Experimental setup used for simultaneous measurement of weight change and conductivity.

was added to the BCY powder to increase electronic conductivity, and the mixture was pressed with a 100 MPa load into pellets of 22.5 mm diameter and ≈2 mm thickness. The BCY-cermet pellets were then sintered at 1550°C for 5 h in an atmosphere of 4% hydrogen and 96% argon. Proton-conducting membranes with and without the addition of metal powder are referred as BCY and BCY-cermet in this paper.

Total and ionic conductivities of SFC were measured as a function of oxygen partial pressure (p_{O_2}) by using conventional four-probe and electron-blocking four-probe methods [17,20]. Figure 1 shows the experimental setup used to determine the conductivity and weight change of the specimens simultaneously. Environments of various p_{O_2} were achieved with premixed gases. Weight of the specimen was determined by a CAHN TG-121 thermogravimeter. Conductivity of the specimen was measured using four-probe method. Oxygen diffusion process in an oxide sample can be described by using Fick's second law:

$$\frac{\partial C}{\partial t} = \mathrm{div}(D \cdot \mathrm{grad}\, C) \qquad [1]$$

where C is the concentration of diffusing substance in the sample. The oxygen chemical diffusion coefficient of an oxide can be derived by fitting the weight/conductivity relaxation data to the solution of Fick's second law with appropriate initial and boundary conditions. Use of a thin-slab specimen of thickness 2l can dramatically simplify the solution. Weight and conductivity relaxation data were fit to the following equations [21] to determine the chemical diffusion coefficient of the SFC sample:

$$\frac{\Delta W(t)}{\Delta W(\infty)} = 1 - \sum_{n=0}^{\infty} \frac{8}{(2n+1)^2\pi^2} \exp\left[-\frac{(2n+1)^2\pi^2 \tilde{D}_{wt} t}{4l^2}\right] \qquad [2.1]$$

$$\frac{\Delta \sigma(t)}{\Delta \sigma(\infty)} = 1 - \sum_{n=0}^{\infty} \frac{8}{(2n+1)^2\pi^2} \exp\left[-\frac{(2n+1)^2\pi^2 \tilde{D}_{el} t}{4l^2}\right] \qquad [2.2]$$

where $\Delta W(t) = W(t) - W(0)$ is the specimen weight change at time t, and $\Delta W(\infty) = W(\infty) - W(0)$ is the weight change at time infinity. Similarly, $\Delta\sigma(t) = \sigma(t) - \sigma(0)$ is the conductivity change at time t, and $\Delta\sigma(\infty) = \sigma(\infty) - \sigma(0)$ is the conductivity change at time infinity. D_{wt} and D_{el} denote the oxygen chemical diffusion coefficient as determined from weight change and conductivity change data, respectively. Oxygen permeation of SFC was determined with a gas-tight cell discussed in Ref. 22. A sintered pellet of SFC was sealed to an yttria-stabilized zirconia (YSZ) crucible with a Pyrex glass seal. Two electrodes were placed on the bottom and side of the YSZ crucible, respectively, to serve as oxygen pump and oxygen sensor. The p_{O_2} inside the cell can be determined from the electromotive force (EMF), E, generated on the side-wall electrodes (sensor) by solving,

$$p_{O_2}^{II} = p_{O_2}^{I} \exp\left(\frac{4FE}{RT}\right) \qquad [3]$$

where $p_{O_2}^{II}$ and $p_{O_2}^{I}$ are the p_{O_2} values inside and outside the gas-tight cell, respectively. Other variables are as usual.

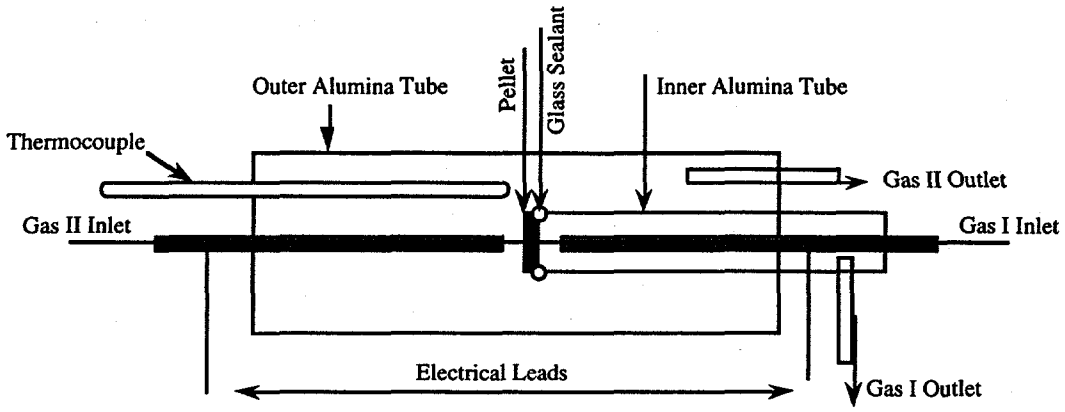

Figure 2. Experimental setup for electrical characterization of BCY proton conductor.

The experimental setup for investigating proton transport in the BCY samples is illustrated in Fig. 2. Platinum mesh (#80) was cut to the appropriate size and attached with platinum paint (Heraeus CL11-5100) to both polished sides of a sintered specimen. The BCY specimen and platinum mesh were then heated to 150°C, held at that temperature for 2 h, and then heated at 850°C for 30 min for conditioning. Subsequently, the BCY specimen was sealed with a glass sealant [23] onto one end of the inner alumina tube for OCV tests. BCY-cermet samples of three thicknesses were tested for hydrogen permeability by using the same setup. 4% hydrogen and 96% argon was used as the feed gas, and 99.999% argon was used as the sweeping gas. Hydrogen flux through the BCY-cermet membrane was measured by gas chromatography.

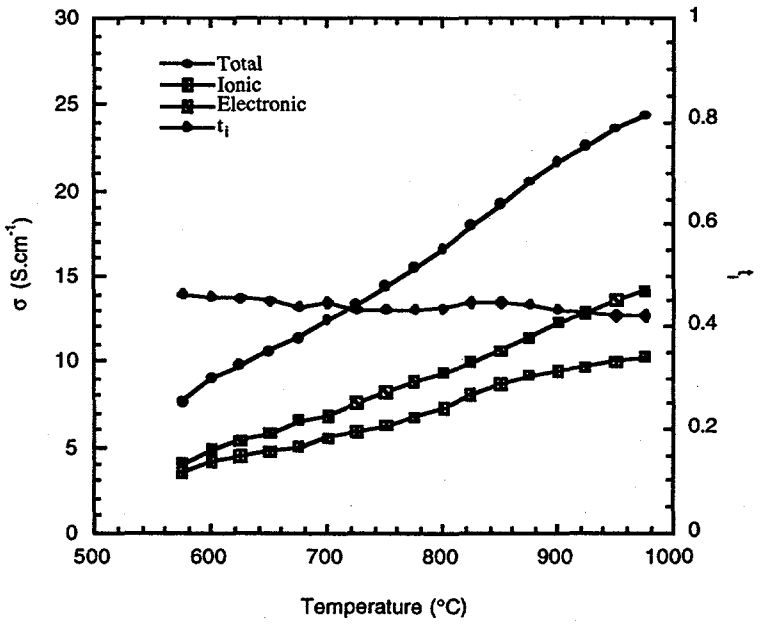

Figure 3. Temperature dependence of total, electronic, and ionic conductivities, and ionic transference number of SFC sample.

RESULTS AND DISCUSSION

Oxygen Ionic Conductor SFC

Using the conventional four-probe and electron-blocking four-probe methods, we measured the total and ionic conductivities of SFC. The ionic transference number can be determined from ionic conductivity divided by total conductivity. The total and ionic conductivities and the ionic transference number of SFC in air are plotted in Fig. 3 as a function of temperature. Conductivities increase with increasing temperature, whereas the ionic transference number is almost independent of temperature. At 800°C in air, the total conductivity and oxygen ionic conductivity are ≈17 and 7 $S \cdot cm^{-1}$, respectively, which leads to an ionic transference number of ≈0.4. This result indicates that the electronic and ionic conductivities of the SFC sample are comparable in value, i.e., their ratio is close to unity. This makes the SFC materials unique among other mixed conductors, in which electronic transference numbers are much greater than ionic transference numbers, or vice versa.

Without considering surface effect, oxygen permeation flux j_{O_2}, through a membrane of thickness L can be calculated from conductivity data [20] as follows:

$$j_{O_2} = \frac{RT}{16F^2L}\int_{p'_{O_2}}^{p''_{O_2}} \sigma_{tot} t_{ion} t_{el} d\ln(p_{O_2}) \qquad [4]$$

where σ_{ion} is total conductivity, t_{ion} is ionic transference number, and t_{el} is electronic transference number. According to Eq. 4, a maximum oxygen flux can be obtained when the electronic and ionic transference numbers are close to each other in value. Therefore, SFC material is an excellent candidate for use as membranes for oxygen separation.

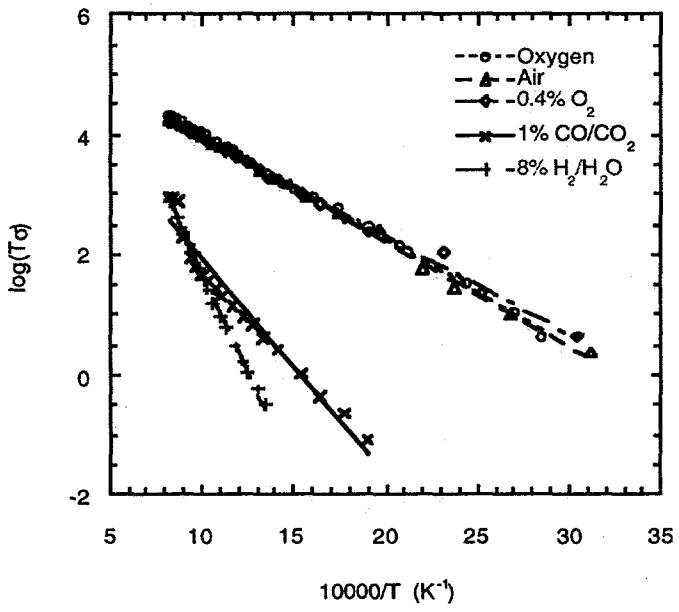

Figure 4. Conductivity of SFC in various environment.

The various p_{O_2} environments were achieved with premixed gases. After switching the surrounding gas, change in weight and conductivity of the specimen was monitored.

Conductivity data was taken after the specimen reached its equilibrium in the new atmosphere. Figure 4 shows $\log(T\cdot\sigma)$ as a function of reciprocal temperature for SFC sample in various oxygen environments. The $\log(T\cdot\sigma)$ vs. reciprocal temperature curves have good linear dependence; therefore, activation energy can be derived from slopes of these curves. Conductivity at 950°C and the activation energy of SFC in various p_{O_2} environments are listed in Table 1. Conductivity increases with increasing p_{O_2}. In high-p_{O_2} environments, activation energy of SFC samples was low, ≈0.35 eV. Activation energy increased with decreasing p_{O_2} in a reducing environment.

Table 1. Conductivity at 950°C and activation energies of SFC in various oxygen atmospheres.

Atmosphere	$\log(p_{O_2})$	σ (S·cm^{-1})	E_a (eV)
100% O_2	0	23.21	0.35
air	-0.678	20.91	0.35
0.4% O_2/Ar	-2.373	18.68	0.34
1% CO/CO_2	-11.5	1.05	0.63
8% H_2/H_2O	-18.2	0.86	1.31

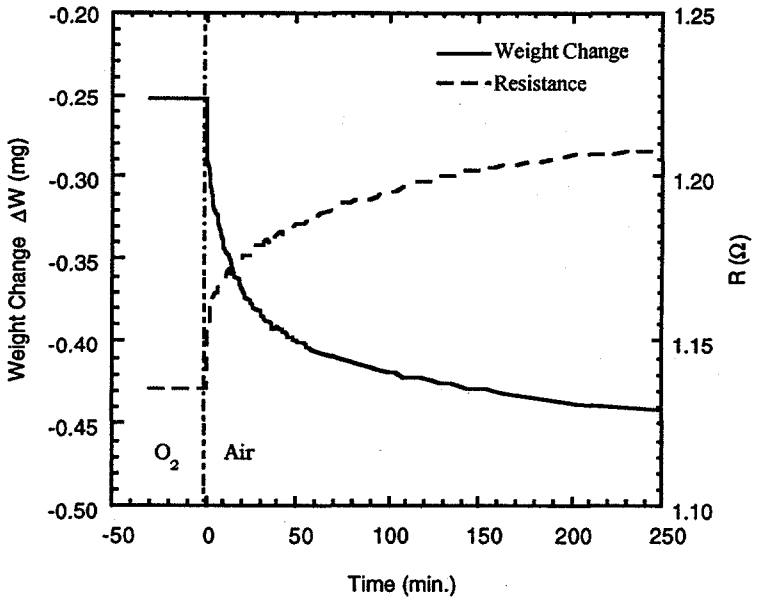

Figure 5. Weight and corresponding resistance relaxation curve for SFC at 950°C after changing surrounding environment from pure O_2 to air.

The weight change and conductivity relaxation data of SFC are shown in Fig. 5 as functions of relaxation time after switching the surrounding atmosphere from 100% pure oxygen to air at 950°C. Weight and conductivity relaxation data were analyzed by least-squares fitting to Eq. 2 with the corresponding geometric parameters of the specimens. The oxygen chemical diffusion coefficient of SFC derived from the weight-relaxation data ($\tilde{D}_{wt}$) and from the conductivity-relaxation data (D_{el}) are listed in Table 2. At 950°C, the oxygen chemical diffusion coefficient of SFC is $\approx 10^{-6}$ cm^2·s^{-1} as determined in relaxation experiments.

Table 2. Oxygen chemical diffusion coefficient of SFC in various oxygen atmospheres at 950°C.

Atmosphere Change	$\Delta\log(p_{O_2})$	$\tilde{D}_{wt}$ ($cm^2 \cdot s^{-1}$)	$\tilde{D}_{el}$ ($cm^2 \cdot s^{-1}$)
100% O_2 to air	-0.678	5.27×10^{-7}	1.21×10^{-6}
air to 0.4% O_2/Ar	-1.695	7.13×10^{-7}	1.64×10^{-6}
0.4% O_2/Ar to air	+1.695	5.38×10^{-6}	5.40×10^{-6}
0.4% O_2/Ar to 1% CO/CO_2	-9.127	1.36×10^{-6}	1.27×10^{-6}
1% CO/CO_2 to 8% H_2/H_2O	-6.700	7.78×10^{-7}	7.18×10^{-6}

Table 3 lists the weight change and corresponding change in oxygen content of SFC with p_{O_2} change at 950°C. Oxygen content in SFC decreases with decreasing p_{O_2} as expected. From Table 3, we observe that the change of oxygen content for SFC is 0.0134 + 0.1529 = 0.1663 while the surrounding atmosphere changed from air to 1% CO/CO_2. This value of oxygen content change is in very good agreement with the value that corresponds to the hematite (Fe_2O_3) to magnetite (Fe_3O_4) transition of iron, $3Fe_2O_3 \Leftrightarrow 2Fe_3O_4 + 0.5O_2$. This implies that Fe ions exist in the 3+ state, and that Sr and Co ions exist in the 2+ state at 950°C in air. Furthermore, SFC can be considered as a solid solution of SrO, Fe_2O_3, and CoO with appropriate mole ratio. This leads to $x = 3$ in the chemical formula of the material at 950°C in air. Oxygen content as a function of p_{O_2} for SFC sample at 950°C is shown in Fig. 6.

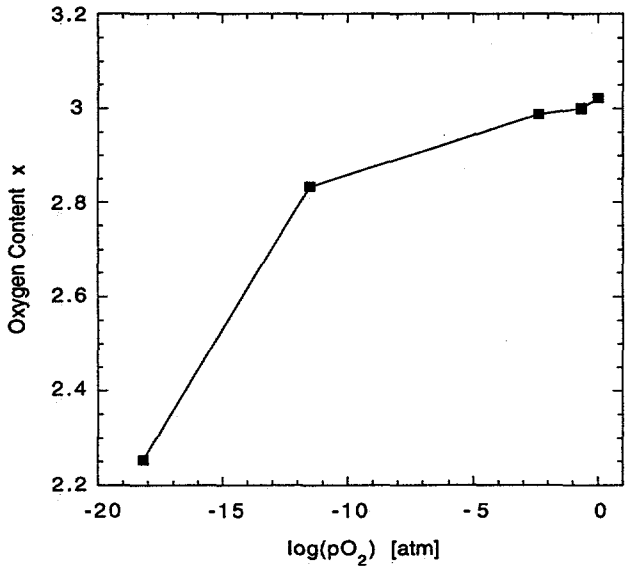

Figure 6. Oxygen content of SFC in environments of various oxygen partial pressures.

Table 3. Weight and corresponding oxygen content change of SFC with p_{O_2} change at 950°C[a].

Atmosphere Change	$\Delta\log(p_{O_2})$	ΔW(mg)	Δx
100% O_2 to air	-0.678	0.2366	0.0211
air to 0.4% O_2/Ar	-1.695	0.1503	0.0134
0.4% O_2/Ar to 1% CO/CO_2	-9.127	1.7153	0.1529
1% CO/CO_2 to 8% H_2/H_2O	-6.700	8.2115	0.7321

[a]Weight of the specimen in air is 0.1549 g.

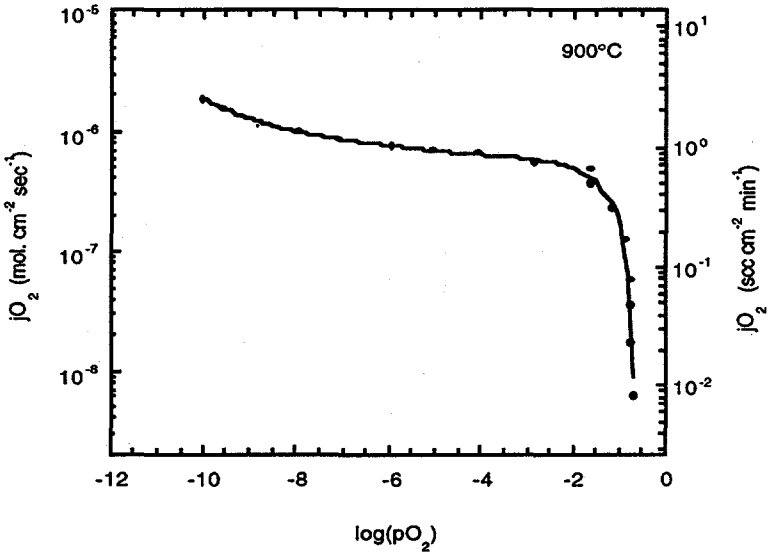

Figure 7. Oxygen permeation flux as a function of oxygen partial pressure, determined with a gas-tight cell.

Oxygen permeability of SFC was determined with a gas-tight cell that was described in our earlier publication [22]. Reducing oxygen environments were achieved by pumping oxygen out of the gas-tight cell. Oxygen permeates through the SFC disk membrane because of the p_{O_2} difference on the two sides of the specimen. Under steady-state conditions, the amount of oxygen that enters the cell (via permeation through the specimen) is equal to that pumped out by the YSZ oxygen pump. Therefore, the flow of oxygen through the specimen can be determined from the current applied to the YSZ oxygen pump. Oxygen permeation flux j_{O_2} is related to the applied current I as follows:

$$j_{O_2} = \frac{I}{4FS} \qquad [5]$$

where S is the effective cross-sectional area of the specimen.

Oxygen permeation flux through a 2.9-mm-thick SFC disk, obtained from Eq. 5, the experimental data of a steady-state pumping current I, and geometric parameters of the specimen, is plotted in Fig. 7 as a function of the p_{O_2} inside the gas-tight cell. Flowing air (p_{O_2} = 0.21 atm) was used as the reference atmosphere during oxygen permeation experiments. Figure 7 shows that j_{O_2} increases dramatically in the range between p_{O_2} = 0.21 and $\approx 10^{-3}$ atm, and its slope becomes flatter when p_{O_2} inside the cell is reduced further. Results on oxygen permeability at various p_{O_2} gradients and temperatures show that j_{O_2} increases, as expected, with temperature and p_{O_2} gradients. At 900°C, oxygen permeability was $\approx$2.5 ssc·cm^{-2}·min^{-1} for a 2.9-mm-thick specimen and increases as membrane thickness decreases.

Sintered thin-wall tubes of SFC were tested in a methane conversion reactor for >1000 h [18,19,23]. Oxygen permeation flux determined from reactor experiments (with tubular SFC membrane) [24] and that determined using a gas-tight electrochemical cell have been plotted in Fig. 8 as a function of temperature. Results from these two experiments are in good agreement.

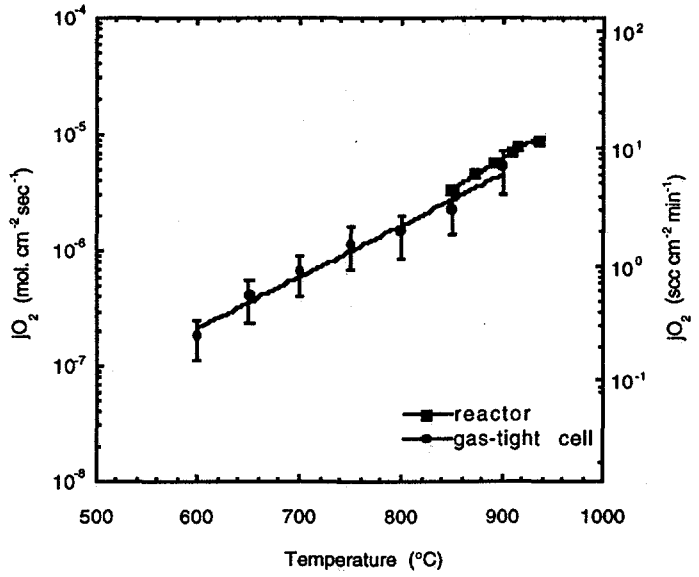

Figure 8. Temperature dependence of oxygen permeation fluxes determined with a gas-tight electrochemical cell and in methane conversion reactor.

Protonic Conductor BCY

Figure 9 shows the total conductivity of BCY in various atmospheres, as determined by impedance spectroscopy. The total conductivity of $BaCe_{0.95}Y_{0.05}O_{3-\delta}$ was low in pure argon, even at high temperatures (≥600°C), but increased slightly with addition of 2% water vapor in the surrounding environment. Total conductivity of BCY was higher in pure oxygen than in pure argon. At low temperatures, addition of water increased the total conductivity, whereas at high temperatures, total conductivity slightly decreased when water vapor was added. Total conductivity of the BCY sample increased from ≈5 x 10^{-3} $\Omega^{-1}\cdot cm^{-1}$ to ≈2 x 10^{-2} $\Omega^{-1}\cdot cm^{-1}$ at 600°C.

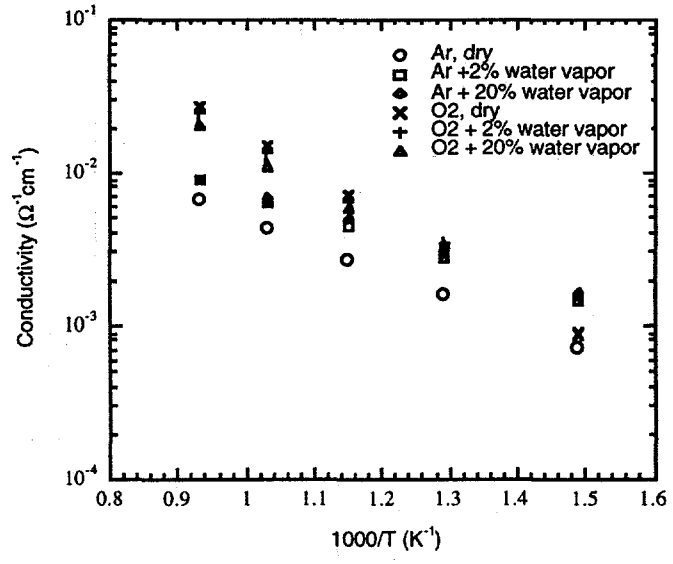

Figure 9. Total conductivity of BCY measured in various atmospheres.

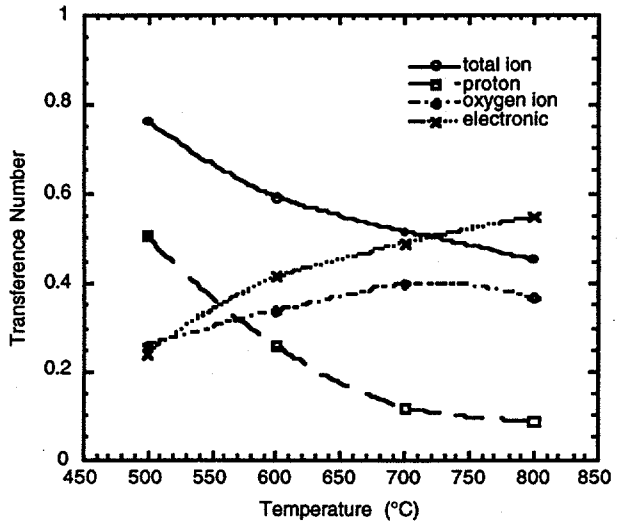

Figure 10. Transference number of BCY as determined in oxygen-containing environment.

Transference numbers in an oxygen-containing atmosphere were determined by using the following concentration cells:

II, O_2 + 2.81% H_2O, Pt|BCY|Pt, N_2 + 8% O_2 + 2.81% H_2O, I [c1]
II, O_2 + 7.38% H_2O, Pt|BCY|Pt, N_2 + 8% O_2 + 2.64% H_2O, I [c2]
II, N_2 + 8% O_2 + 7.38% H_2O, Pt|BCY|Pt, N_2 + 2.81% H_2O, I [c3]

As shown in Table 4, the measured OCVs of Cell 1 decreased as temperature increased, indicating that the electronic transference number increases with temperature. In Cell 2, where the OCV was solely due to the partial-pressure difference of water vapor, the OCVs are directly related to the protonic transference number according to the following equation [23]:

$$V_{OC} = \frac{RT}{4F}\left[t_{ion} \ln\left(\frac{p^{II}_{O_2}}{p^{I}_{O_2}}\right) - 2t_{H^+} \ln\left(\frac{p^{II}_{H_2O}}{p^{I}_{H_2O}}\right)\right] \quad [6]$$

where $t_{ion} = t_{H^+} + t_{O^{2-}}$ is the ionic transference number. The obtained transference numbers are plotted in Fig. 10, which shows that the protonic transference number decreases, whereas the electronic transference number increases with increasing temperature.

Table 4. Open-cell voltages (mV) of oxygen/water vapor concentration cells at various temperatures.

Temperature (°C)	Cell 1	Cell 2	Cell 3
500	32.0	14.8	-48.2
600	28.0	19.9	-36.8
700	27.2	22.1	-31.3
800	26.4	22.3	-29.7

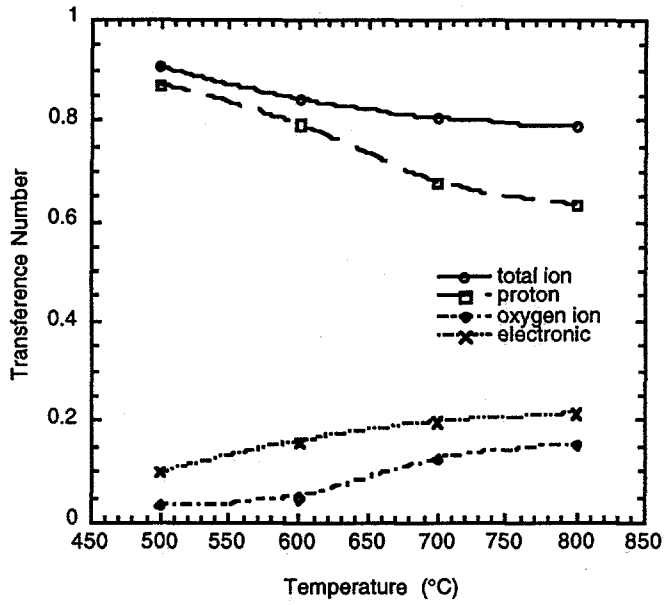

Figure 11. Transference number of BCY as determined in hydrogen-containing environment.

Transference numbers in hydrogen/water vapor atmospheres were studied by employing the following cells:

II, N_2 + 4% H_2 + 2.64% H_2O, Pt|BCY|Pt, N_2 + 0.488% H_2 + 2.64% H_2O, I [c4]
II, N_2 + 4% H_2 + 7.38% H_2O, Pt|BCY|Pt, N_2 + 0.488% H_2 + 2.64% H_2O, I [c5]
II, N_2 + 0.488% H_2 + 7.38% H_2O, Pt|BCY|Pt, N_2 + 4% H_2 + 2.64% H_2O, I [c6]

The obtained OCVs are listed in Table 5, and the ionic transference numbers were derived by solving the following equation [23]:

$$V_{OC} = \frac{RT}{4F}\left[-t_{ion}\ln\left(\frac{p^{II}_{H_2}}{p^{I}_{H_2}}\right) + t_{O^{2-}}\ln\left(\frac{p^{II}_{H_2O}}{p^{I}_{H_2O}}\right)\right] \quad [7]$$

The obtained transference numbers are plotted in Fig. 11. Again, the protonic transference number decreases, whereas the electronic transference number increases with increasing temperature. The protonic transference number decreases from 0.87 to 0.63, whereas the oxygen transference number increases from 0.03 to 0.15 as temperature increases from 600 to 800°C in the hydrogen/water vapor atmospheres.

Table 5. Open-cell voltages (mV) of hydrogen/water vapor concentration cells at various temperatures.

Temperature (°C)	Cell 4	Cell 5	Cell 6
500	-63.13	-62.01	64.02
600	-66.43	-64.48	68.14
700	-70.55	-65.17	75.57
800	-76.39	-69.11	83.26

Analogous to oxygen permeation flux (given in Eq. 2), the hydrogen permeation flux through a bulk-property-controlled proton-permeable membrane can be written as follows:

$$j_{H_2} = \frac{RT}{4F^2L}\int_{p'_{H_2}}^{p''_{H_2}} \sigma_{tot} t_{ion} t_{el} d\ln(p_{H_2}) \qquad [8]$$

where σ_{tot} is the total conductivity, t_{ion} is the ionic transference number, and t_{el} is the electronic transference number. Other parameters have their usual meaning.

Under constant hydrogen partial pressure difference, hydrogen flux through a membrane would be optimized if the electronic and protonic transference numbers of the composite BCY material were both ≈0.5. In a hydrogen-containing environment, the protonic transference number of BCY is 3-10 times greater than the electronic transference number. To increase the electronic conductivity of the material, we added metal powder to BCY material to form a composite membrane. The hydrogen permeation rate for such composite membranes of three thicknesses is shown in Fig. 12 as a function of temperature. Plotting the permeation rate against the inverse of sample thickness [25] indicates that the ambipolar conductivity increased while the interfacial polarization resistance decreased dramatically as temperature increased from 600 to 800°C. At 800°C, bulk resistance is much greater than interfacial resistance (for sample thickness of >1 mm), whereas interfacial resistance dominates at low temperature (<600°C). This implies that the permeation rate could be increased by reducing the membrane thickness for gas separations that are performed at high temperatures but would be less effective at lower temperatures.

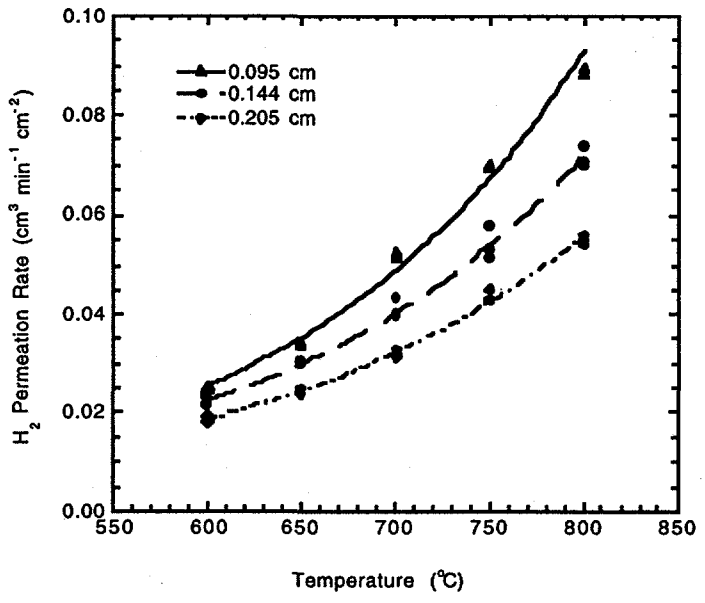

Figure 12. Temperature and thickness dependence of hydrogen permeation rates through BCY-cermet membranes with 4% H_2 (balanced with argon) as feed gas; sweep gas was argon.

CONCLUSIONS

We developed a mixed-conducting ceramic membrane that exhibits combined high electronic and oxygen ionic conductivities and that has electronic and ionic transference numbers that are comparable to each other, making it unique among other mixed conductors. Oxygen permeability of the Sr-Fe-Co oxide (SFC) membrane is high, making this material a good candidate for use in membranes for oxygen separation applications. Conductivities increase with increasing temperature, whereas the ionic transference number is almost independent of temperature. At 800°C in air, total conductivity and oxygen ionic conductivity are ≈17 and 7 $S \cdot cm^{-1}$, respectively, which leads to an ionic transference number of ≈0.4. Conductivity of SFC increases with increasing p_{O_2}. In high-p_{O_2} environments, activation energy of SFC sample was low, ≈0.35 eV. Activation energy increases with decreasing p_{O_2} in the further reducing environment. At 950°C, oxygen chemical diffusion coefficient of SFC is $\approx 10^{-6}$ $cm^2 \cdot s^{-1}$ as determined in relaxation experiments. Direct measurement of oxygen permeation flux with a gas-tight electrochemical cell agrees well with values obtained from other oxygen permeation experiments and with values calculated from conductivity data. At 900°C, oxygen permeation flux, as determined with a gas-tight electrochemical cell, was ≈2.5 $scc \cdot cm^{-2} \cdot min^{-1}$ for a 2.9-mm-thick specimen. Oxygen permeability of the SFC membranes increases with increasing temperature and decreasing membrane thickness.

Hydrogen permeable Y-doped $BaCeO_{3-\delta}$ (BCY) material was studied in various atmospheres. Conductivity of BCY increases with increasing temperature. At 600°C, total conductivity of BCY is $\approx 5 \times 10^{-3}$ to 2×10^{-2} $\Omega^{-1} \cdot cm^{-1}$. As determined in open-cell voltage experiments, the ionic transference number of BCY decreased from 0.87 to 0.63 and the oxygen transference number increased from 0.03 to 0.15 as temperature increased from 600 to 800°C. BCY-cermet composite membranes were developed. A hydrogen permeation flux of ≈0.1 $scc \cdot cm^{-2} \cdot min^{-1}$ was observed in a disk membrane of 0.095 cm thickness. Measurement of hydrogen permeation rate through BCY-cermet membranes showed that interfacial polarization is significant at lower temperatures ($T < 600$°C) but decreases dramatically at higher temperatures. Decreasing the membrane thickness may increase the permeation rate for high-temperature separations, but would have less effect on separations at lower temperatures.

ACKNOWLEDGMENTS

This work was supported by the U.S. Department of Energy, Federal Energy Technology Center, under Contract W-31-109-Eng-38. We thank Dr. J.-H. Park for his help in the weight/conductivity relaxation experiments.

REFERENCES:

1. H. Iwahara, T. Esaka, H. Uchida, and N. Maeda, *Solid State Ionics*, **3/4**, 359 (1981).
2. T. Yajima, H. Suzuki, T. Yogo, and H. Iwahara, *Solid State Ionics*, **51**, 101 (1992).
3. H. Iwahara, *Solid State Ionics*, **77**, 289 (1995).
4. J. F. Liu and A. S. Nowick, *Mater. Res. Soc. Symp. Proc.*, **210**, 673 (1991).
5. N. Bonanos, *Solid State Ionics*, **53-56**, 967 (1992).
6. N. Taniguchi, K. Hatoh, J. Niikura, and T. Gamo, *Solid State Ionics*, **53-56**, 998 (1992).
7. D. A. Steveson, N. Jiang, R. M. Buchanan, and F. E. G. Henn, *Solid State Ionics*, **62**, 279 (1993).
8. Y. Teraoka, H. Zhang, S. Furukawa, and N. Yamazoe, *Chem. Lett.*, 1743 (1985).

9. Y. Teraoka, H. Zhang, K. Okamoto, and N. Yamazoe, *Mater. Res. Bull.*, **23**, 51 (1988).
10. Y. Nigara, J. Mizusaki, and M. Ishigame, *Solid State Ionics*, **79**, 208 (1995).
11. H. Arashi, H. Naito, and M. Nakata, *Solid State Ionics*, **76**, 315 (1995).
12. R. H. E. Van Doorn, H. Kruidhof, H. J. M. Bouwmeester, and A. J. Burggraaf, *Mater. Res. Soc. Symp. Proc.*, **369**, 377 (1991).
13. Y. Teraoka, T. Nobunaga, K. Okamoto, N. Miura, and N. Yamazoe, *Solid State Ionics*, **48**, 207 (1991).
14. H. W. Brinkman, H. Kruidhof, and A. J. Burgraaf, *Solid State Ionics*, **68**, 173 (1994).
15. U. Balachandran, S. L. Morissette, J. T. Dusek, R. L. Mieville, R. B. Poeppel, M. S. Kleefisch, S. Pei, T. P. Kobylinski, and C. A. Udovich, *Proc. Coal Liquefaction and Gas Conversion Contractor Review Conf.*, S. Rogers et al., eds., **Vol. 1**, pp. 138-160, U.S. Dept. of Energy, Pittsburgh Energy Technology Center (1993).
16. U. Balachandran, M. S. Kleefisch, T. P. Kobylinski, S. L. Morissette, S. Pei, U.S. Patent 5580497, Dec. 1996.
17. B. Ma, J.-H. Park, C. U. Segre, and U. Balachandran, *Mater. Res. Soc. Symp. Proc.*, **393**, 49 (1995).
18. U. Balachandran, T. J. Dusek, S. M. Sweeney, R. B. Poeppel, R. L. Mieville, P. S. Maiya, M. S. Kleefisch, S. Pei, T. P. Kobylinski, C. A. Udovich, and A. C. Bose, *Am. Ceram. Soc. Bull.*, **74**, 71 (1995).
19. U. Balachandran, J. T. Dusek, P. S. Maiya, B. Ma, R. L. Mieville, M. S. Kleefisch, and C. A. Udovich, *Catalysis Today*, **36**, 265 (1997).
20. B. Ma, U. Balachandran, and J.-H. Park, *J. Electrochem. Soc.*, **143**, 1736 (1996).
21. B. Ma, J.-H. Park, and U. Balachandran, *J. Electrochem. Soc.*, **144**, 2816 (1997).
22. B. Ma, U. Balachandran, C.-C. Chao, and J.-H. Park, *Ceram. Trans. Series Am. Ceram. Soc.*, **Vol. 73**, p. 169 (Westerville, OH, 1997).
23. J. Guan, S. E. Dorris, U. Balachandran, and M. Liu, *Solid State Ionics*, **100**, 45 (1997).
24. P. S. Maiya, U. Balachandran, J. T. Dusek, R. L. Mieville, M. S. Kleefisch, and C. A. Udovich, *Solid State Ionics*, **99**, 1 (1997).
25. J. Guan, S. E. Dorris, U. Balachandran, and M. Liu, presented at Symp. on Electrochemistry of Glass and Ceramics, 100th Annual Meeting and Exposition of American Ceramic Society, Cincinnati, May 3-6, 1998.